



Low-frequency variability of the Mediterranean undercurrent off Galicia, northwestern Iberian Peninsula

J. García Lafuente ^{a,*}, J.C. Sánchez Garrido ^{a,b}, G. Díaz del Río ^c, F. Criado Aldeanueva ^a, D. Marcote ^c, A. Sánchez Román ^a

^a Grupo de Oceanografía Física, University of Málaga, Málaga, Spain

^b Grupo de Puertos y Costas, University of Granada, Granada, Spain

^c Laboratorio Oceanográfico de A Coruña, Instituto Español de Oceanografía, A Coruña, Spain

ARTICLE INFO

Article history:

Received 13 February 2007

Received in revised form 20 February 2008

Accepted 21 February 2008

Available online 6 March 2008

Keywords:

Mediterranean vein

Seasonal variations

Mesoscale features

Wind stress

Upwelling

Artabro Gulf (NW Iberian Peninsula)

ABSTRACT

The variability of the Mediterranean flow off Galicia, at the northwestern corner of the Iberian Peninsula has been investigated by means of a four-month time series of velocity and temperature collected at two different sites in the depth range of the Mediterranean water influence. The time series cover the initial and development phases of the seasonal upwelling and indicate that the vein of Mediterranean water is raised and, probably, displaced shoreward as the upwelling sets up. Data show that the vein flows around 100 m shallower in September, when the seasonal upwelling is developed the most, than in May, before the upwelling season starts. The raising is not achieved in a smooth and continuous manner but undergoing noticeable mesoscale variability that has been assigned to vertical and horizontal (inshore-offshore) displacements of the vein, whose origin is partially related to the variability of the large-scale wind field. The footprint that the internal tide leaves in the temperature records at M2 tidal frequency in the instruments placed above and below the core of the Mediterranean vein along with the registered temperature have been used to diagnose the subtidal displacements of the vein.

© 2008 Elsevier B.V. All rights reserved.

1. Introduction

The Mediterranean water leaves the Mediterranean Sea by overflowing the sills of the Strait of Gibraltar at a depth of around 300 m. The typically 1 Sv (Sverdrup, $1 \text{ Sv} = 10^6 \text{ m}^3 \text{ s}^{-1}$) of Mediterranean outflow represents an input of warm and salty water (potential temperature $\theta = 13^\circ \text{C}$ and salinity $S = 38.4$ units of the Practical Salinity Scale at the source point) into the Atlantic Ocean that sinks to depths of around 800 to 1200 m where it finds its equilibrium depth (Ambar and Howe, 1979). In the Gulf of Cadiz the outflow splits into two-cores and, nearby 9°W , it has increased its volume transport by a factor of nearly 3 due to the entrainment of the overlying Eastern North Atlantic Central Water-ENACW—(Baringer and

Price, 1997). In Cape St-Vincent the Mediterranean current veers to flow northwards along the western Iberian Peninsula. The upper core, characterised by a relative maximum of θ , is found at around 800 m depth with θ/S representative values of $13.0^\circ \text{C}/36.4$, respectively, while the lower core is located at around 1200 m with $\theta \sim 12.2^\circ \text{C}$ and $S \sim 36.6$ (Ambar and Howe, 1979).

The area near Cape St-Vincent is prone for Meddy formation (Bower et al., 1997; Cherubin et al., 2000) thus diverting a considerable amount of Mediterranean water towards the eastern North Atlantic in detriment of the northward flowing branch passing through the gateway between Goringe Bank and the Cape (Iorga and Lozier, 1999). This branch proceeds into the Tagus basin, a place of noticeable mesoscale variability where the presence of Estremadura promontory to the north favours a general cyclonic circulation and further losses of Mediterranean water to the open ocean (Daniault et al., 1994) as well as the generation of Meddies (Ambar et al., 2008). Actually, the

* Corresponding author. Grupo de Oceanografía Física, Dpt. of Applied Physics II, ETSI Telecomunicación, Campus de Teatinos s/n, University of Málaga, E29071, Spain. Tel.: +34 952 132721; fax: +34 952 131355.

E-mail address: glafuente@ctima.uma.es (J. García Lafuente).

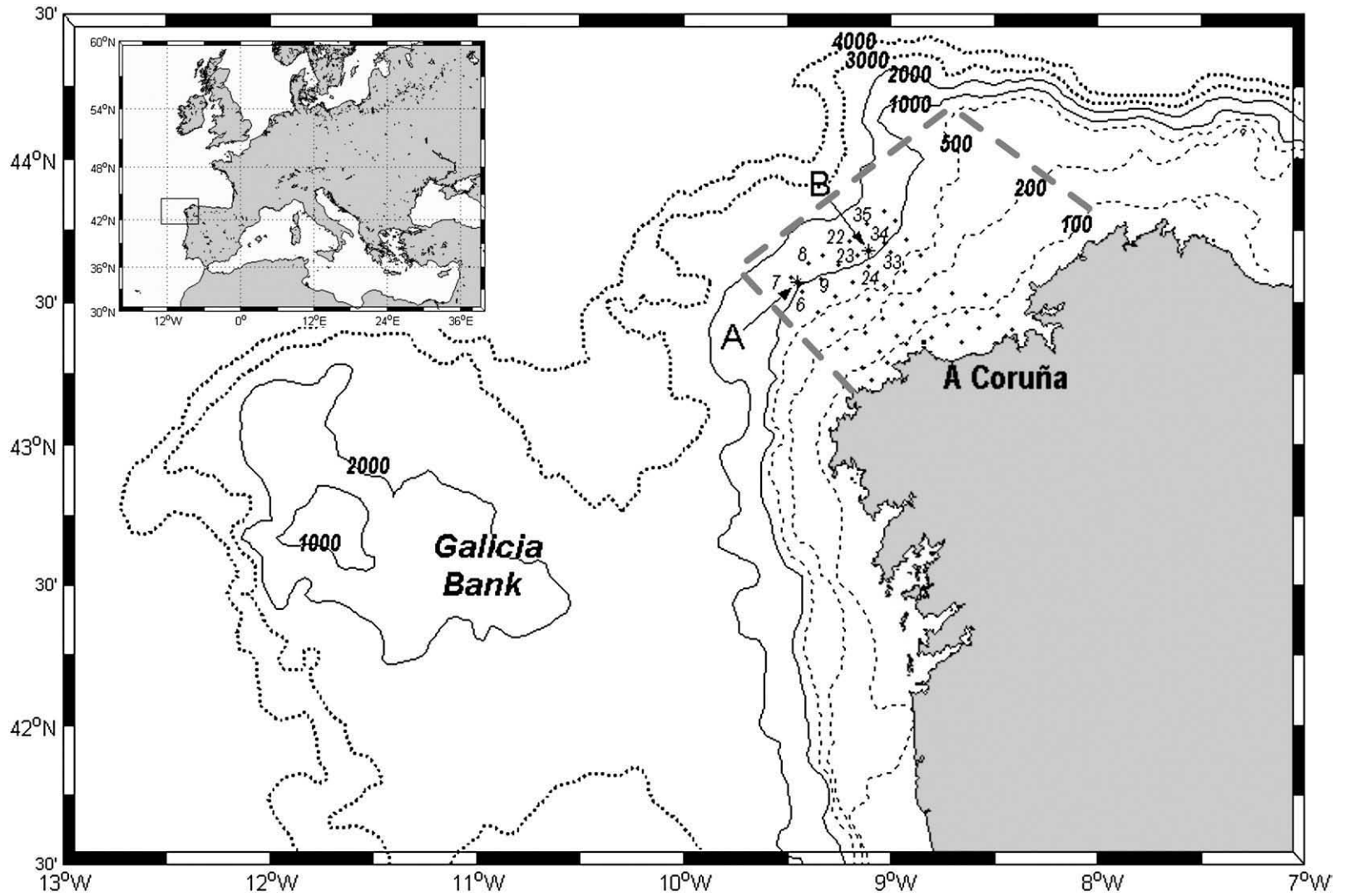


Fig. 1. Map of the area showing the bathymetry and the position of the mooring lines A and B (asterisks). Dashed grey line shows the Artabo Gulf area and dots indicate the location of the CTD stations in surveys ARTABRO1 and ARTABRO2. Casts used to obtain the spatially-averaged temperature and salinity profiles in sites A and B have been labelled. The insert in the upper left corner situates the area of study.

formation of Meddies is not exclusive of these areas. According to Paillet et al. (1999), they can be shed anywhere from the north-going Mediterranean flow during its path along the western façade of the Iberian Peninsula and even further north, as seemed to be the case of Meddy Ulla reported by Paillet et al. (2002) which was probably generated off northwest Galicia. At around 42°N, north of Tagus basin, the Mediterranean flow bifurcates intermittently into two branches (Mazé et al., 1997), one branch flowing west of Galicia bank (Fig. 1) and the other moving north along the continental slope of the Iberian Peninsula. This part of the flow (Mediterranean vein, MV, hereinafter) reaches the northwestern corner of the Peninsula and turns to the right into the Bay of Biscay (Iorga and Lozier, 1999). The motion around the Galicia continental slope is accompanied by a widening of the MV and a noticeable erosion of its salinity

signature to the point that it is hardly distinguishable at 7°W, east of Cape Ortegal (Daniault et al., 1994). These authors indicate that the core of highest salinity in the Mediterranean vein has decreased by 0.4 units and has risen from 1250 m to around 1000 m from Cape St-Vincent to Cape Finisterre.

The two-cores structure of the Mediterranean water observed in the Gulf of Cádiz fades out downstream. Again, Cape St-Vincent seems to be a critical region where the upper core either detaches from the north-moving coastally trapped flow, or undergoes strong erosion (Daniault et al., 1994). In any case, the separated core structure sometimes found in a single vertical profile is lost although the relative maximum of potential temperature and salinity are located at different depths, as a reminiscence of the double-core configuration of the flow in the Gulf of Cádiz. In the Artabro Gulf off the northwestern tip of Galicia where the present study focus on

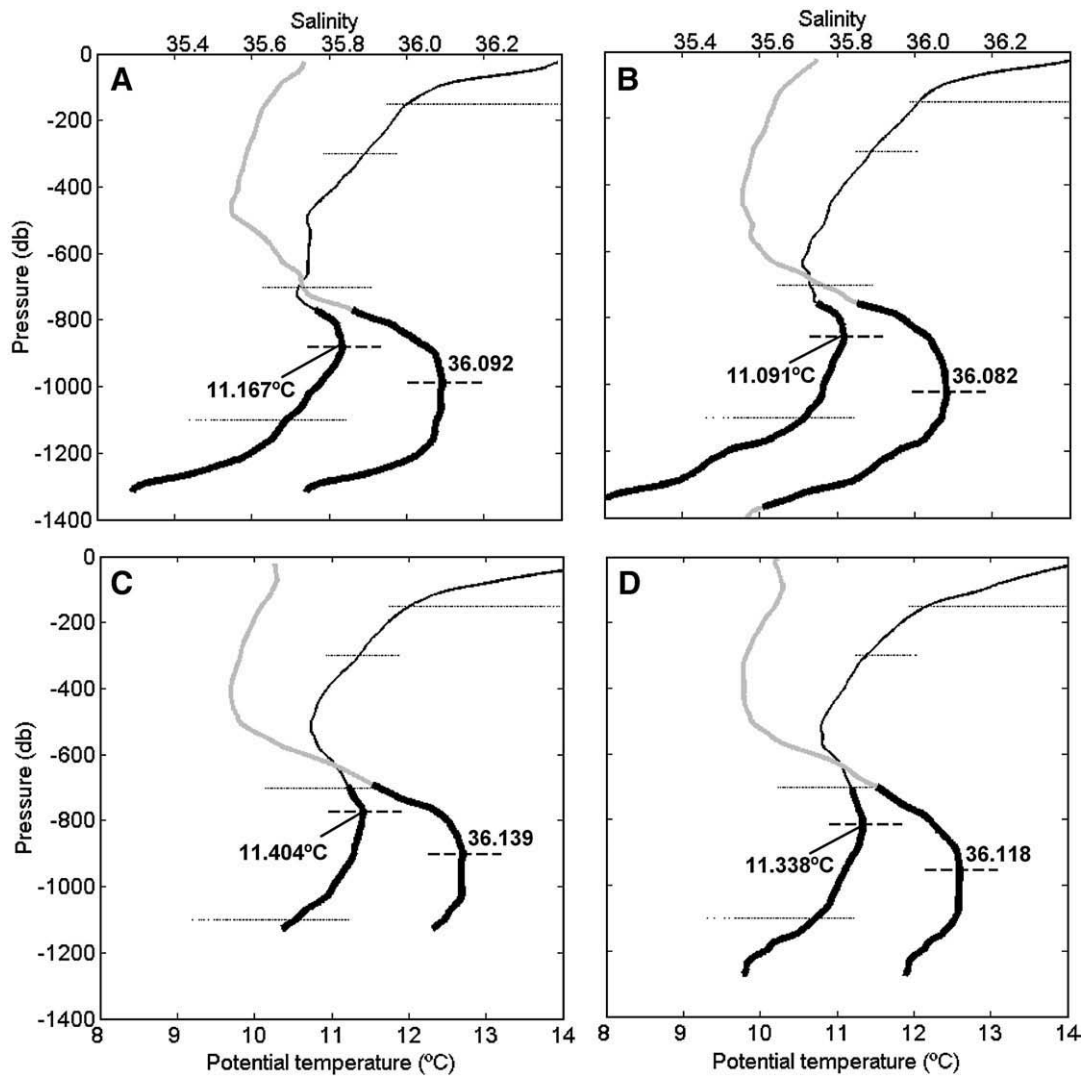


Fig. 2. Spatially averaged temperature and salinity profiles in site A (panel A for May and C for September) and B (panel B for May and D for September). In all panels, the solid black line is potential temperature (scale at the bottom) and the grey line is salinity (scale at the top). The depths of maximum potential temperature and salinity of the Mediterranean water are indicated by solid horizontal segments in each panel. Dots illustrate the range of temperature registered by the different instruments. The thick portion of the temperature and salinity profiles indicate the depth range for which the proportion of Mediterranean water exceeds 40% according to the mixing analysis explained in the text. Numbers indicate the maximum of potential temperature and salinity in each panel.

(ArG hereinafter, see Fig. 1), the relative maximum of potential temperature is found at around 800 m depth while that of salinity is around 1000 m (Díaz del Río, 2006; see also Fig. 2).

The oceanic circulation off the western Iberian Peninsula constitutes a good example of the marked seasonality of the mid-latitude eastern boundary currents in the world ocean. It is driven by the Azores atmospheric high that extends northwards in summer and reduces its size in winter, inducing a well defined seasonal pattern of the wind field along western Iberia. The winter appearance of the Poleward Current flowing northwards at the surface along the Portuguese coast (Frouin et al., 1990; Haynes and Barton, 1990, Torres et al., 2003) and its, at least, subsequent partial replacement by the equatorward upwelling jet during the upwelling season from May to October (Wooster et al., 1976; Fiúza et al., 1982; Haynes et al., 1993; Peliz and Fiúza, 1999; Torres et al., 2003) is a good example of this seasonality that modifies the relative abundance of Atlantic central water masses in the area. In the ArG, Díaz del Río (2006) showed that the Eastern North Atlantic Central Water (ENACW) of subtropical origin advected by the Poleward current is progressively replaced by the colder ENACW of subpolar origin as the upwelling season sets up. The possible seasonal fluctuations of the underlying MV and of its dynamical features, such as the bifurcation at around 42°N, have not been explicitly addressed in the literature although they have been occasionally mentioned by some authors (Mazé et al., 1997; Ambar et al., 2002). A cause-effect relationship for these fluctuations has not been established yet. They could be partially the signature of the distinguishable seasonal cycle observed in the hydrological properties of the Mediterranean water in the sills of Gibraltar, related to the winter formation of Western Mediterranean Deep Water in the Mediterranean Sea (García Lafuente et al., 2007), but they might be a remote conse-

quence of the development of the seasonal upwelling off western Iberia as well.

The bump-like footprint left by the Mediterranean water in the profiles of temperature and salinity at depths around 1000 m in the eastern North-Atlantic can be used to monitor the properties of the MV and their mesoscale to long-term variability. On the other hand, tidal dynamics in the ArG off Galicia exhibits an important bottom intensification (García Lafuente et al., 2006) related to the supercritical bottom topography (topographic gradient greater than the slope of the internal tidal beams) of the continental slope at the depth where the vein flows. The vertical isopycnals displacement of the internal tide induces noticeable oscillations of local temperature/salinity in the depth range under the influence of the MV that can also be used to diagnose displacements of the vein at lower-than-tidal frequencies. In this work we analyse Conductivity–Temperature–Depth (CTD) casts and time series of temperature and velocity collected in the ArG to investigate the mesoscale variability of the MV as it moves through the area.

2. Data acquisition and processing

As part of the program “Study of the Coastal Circulation”, funded by the Instituto Español de Oceanografía, two mooring lines with 4 currentmeters each were deployed in the ArG at 43°34.24′N, 9°26.86′W in water depth of 1170 m (site A hereinafter) and at 43°40.90′N, 9°06.56′W in water depth of 1180 m (site B), respectively. The common period of sampling was from May 15, 1996 at 15:00 UTM to September 12, 1996 at 10:00 UTM, providing a 120-day long time series of velocity and water temperature sampled every 30 min. The instruments were placed at the nominal depths of 150 m (depth #1, in the near surface layer), 300 m (depth #2 in the ENACW layer), 700 m (depth #3, above the MV core near the depth of

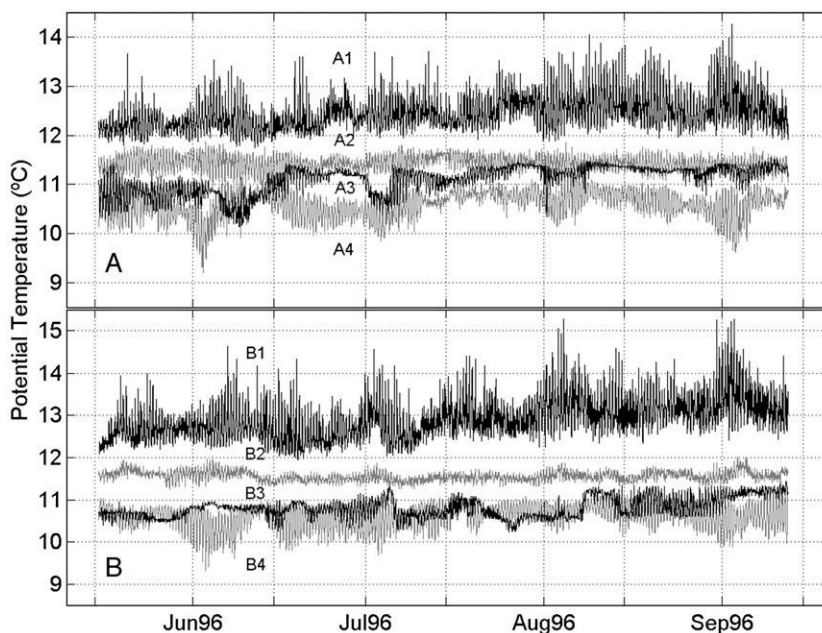


Fig. 3. Time series of potential temperature in the four sampled depths in site A (upper panel) and B (lower panel).

local minimum temperature, see Fig. 2) and 1100 m (depth #4 near the bottom layer, below the MV core). Throughout the paper we identify the stations by a code formed by a letter for the site and a number for the depth: A3 is station in site A at depth #3. Two oceanographic surveys consisting of CTD casts were carried out at the beginning (May 1996, ARTABRO1 survey) and at the end (September 1996, ARTABRO2 survey) of the mooring deployment. The location of the CTD stations is shown in Fig. 1.

Fig. 3 presents the time series of potential temperature in both positions computed using the constant value of salinity $S=36$. The higher frequency fluctuations observable in these plots are forced by tides, which are the main source of variability. The amplitude of the temperature oscillation at the semidiurnal frequency M2 ranged from $0.05\text{ }^{\circ}\text{C}$ in B2 to $0.27\text{ }^{\circ}\text{C}$ in B4 (García Lafuente et al., 2006), with clear bottom intensification. The amplitude changes with time, a fact that is readily shown using the S-transform, a method for dealing with non-stationary signals of time-varying amplitude and phase (Stockwell et al., 1996; Emery and Thompson, 1997). This transform computes the local spectrum of a time series and provides the amplitude and phase of the different harmonics (or “voices”) in the original signal, which are slowly-varying functions of time. The voice at frequency f_0 is then written as

$$X(f_0, t) = A(f_0, t) \cos(2\pi f_0 t + \phi(f_0, t)). \quad (1)$$

Amplitudes can be contoured in a time-frequency plot such that of Fig. 4. Contours show maximum amplitude for semidiurnal frequency (voice M2 mainly) and highlights the

intermittent nature of the internal tide, more evident in stations A3 and B3 at depth #3 than in A4 or B4. As explained in Section 3.2, the dissimilar pattern of intermittence in depths #3 and #4 at the same site can be ascribed to low frequency motions of the MV and, therefore, to diagnose its mesoscale variability.

Wind data from the 40-years re-analysis project of the European Centre for Medium-Range Weather Forecasts (ERA-40, ECMWF) have been retrieved for the point 42.5N, 10.0W and their 8 adjacent grid points, which cover the area of study with an spatial resolution of 2.5° . These data have been used to quantify the magnitude of the upwelling during the upwelling season and to look for relationships between the upwelling indicators (wind stress, wind stress curl) and the mesoscale fluctuations of the MV. Since the spatial resolution of the ECMWF wind data is not excessively dense, we have focused on the sign (positive or negative) of the wind stress curl, which is thought to be representative of the basin, to search for the correlations.

3. Results and discussion

3.1. CTD observations

In order to investigate the variability of the MV, the CTD profiles from stations in the neighbourhood of sites A and B collected during ARTABRO1 and ARTABRO2 surveys have been averaged spatially. The selected stations were 6, 7, 8 and 9 for site A and 22, 23, 24, 33, 34 and 35 for site B (Fig. 1). The mean temperature and salinity profiles in each site and survey are shown in Fig. 2.

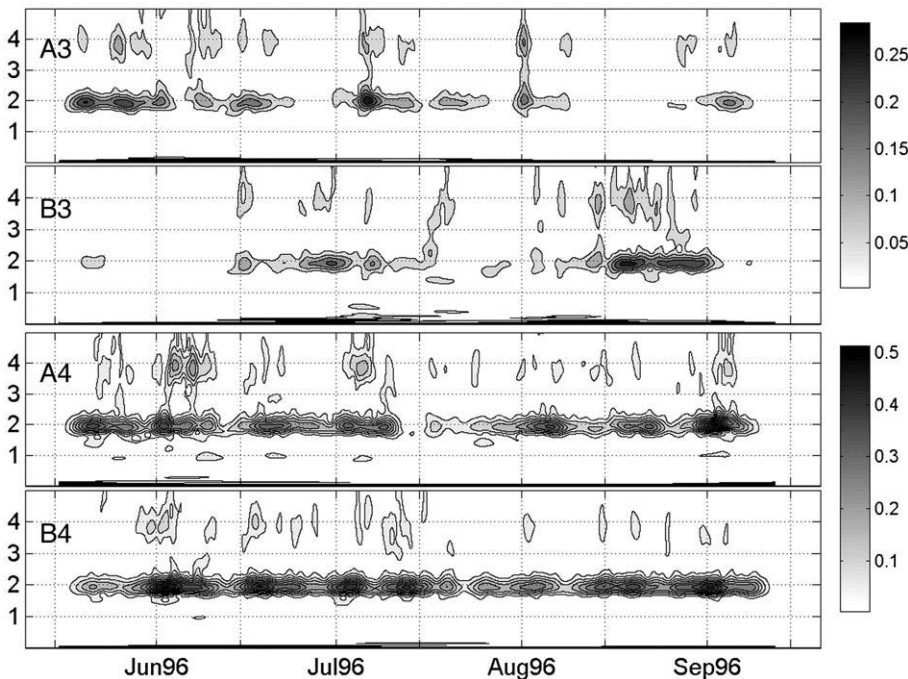


Fig. 4. Contours of amplitude derived from the S-spectrum of temperature observations in stations A3, B3, A4 and B4 (from top to bottom). Y-axis is frequency in cycles per day (cpd). The amplitude scale for stations of level 3 (top panels) is half the scale for stations of level 4 (bottom panels). Most of the energy concentrates in the semidiurnal frequency and in the subinertial range, not well resolved in the analysis. The intermittency of amplitude in stations A3 and B3 is indicative of the proximity of these stations to depths of local extremes of potential temperature. The signal in stations A4 and B4 is more steady in time.

At the time of ARTABRO1 in May, the temperature in site A decreased with depth until 500 m, then it remained nearly constant until 650 m to decrease again to the relative minimum of 10.6 °C at around 720 m in the vicinity of A3. From this depth downwards, the temperature increased until the relative maximum of 11.17 °C within the MV. Temperature profile at point B (Fig. 2B) exhibits similar behaviour although the interval of nearly constant temperature does not exist and the relative maximum is slightly lower (11.09 °C). In September during ARTABRO2 the relative maximum of temperature was 110 m shallower in A and 40 m in B than in May and their numerical values higher (Fig. 2C–D). The relative maximum of salinity is always deeper than that of temperature and it is shallower (100 m in A, 50 m in B) and somewhat greater in September as well. The above referred depths are hardly influenced by internal waves because the amplitude of these waves is not expected to exceed a few meters (order of ten meters). Moreover, the spatially averaging process tends to cancel out the vertical tidal oscillations.

Fig. 5 displays the T–S diagram for both cruises. To obtain information about changes in the thickness of the MV, we have carried out an analysis of water composition using the reference points indicated in the diagram. Point (a) represents the upper limit of the ENACW of subpolar origin (or the lower limit of the ENACW of subtropical origin when present) and is characterised by the pair [12.2, 35.66] for potential temperature and salinity, according to Harvey (1982). Point (b) is the lower end of the ENACW of subpolar origin characterised by the pair [8.56, 35.23] according to Castro et al. (1998). Point (c) is [12.2, 36.6] that identifies the lower core of Mediterranean water in Cape St-Vincent according to Ambar and Howe (1979). Finally, point (d) [3.5, 34.89] corresponds to the Labrador Sea water according to Talley and MacCartney (1982) and Cunningham and Haine (1995). Using points (a, b, c) and (b, c, d) as apices of mixing triangles, we have computed the fraction of Mediterranean water (relative to their T–S characteristics in Cape St-Vincent) in each CTD sample, which has been used to identify the depth interval with fraction greater

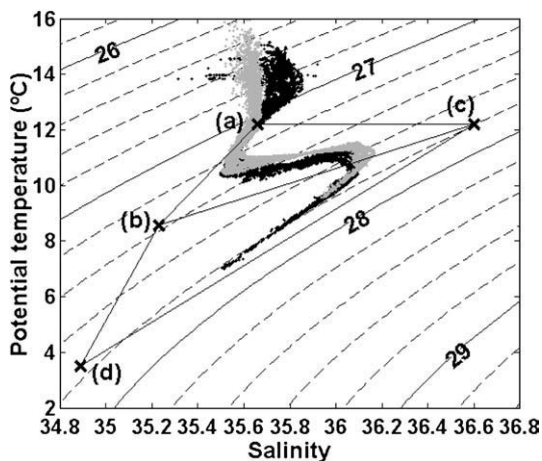


Fig. 5. Potential temperature – salinity diagram of the CTD observations collected during ARTABRO1 (black dots) and ARTABRO2 (grey dots) surveys. Letters in brackets designate the apices of the mixing triangles used to determine the proportion of Mediterranean water.

than a given percentage. In Fig. 2 the depth range with fraction greater than 40% has been marked with thick lines. This value, though arbitrary, helps compare the vertical reach of Mediterranean water in both surveys and shows that the upper limit of 40%-Mediterranean water was 80 m shallower in A (60 m in B) in September, in agreement with the vertical displacements of relative temperature and salinity maxima. It also helps to roughly define the “depth range of Mediterranean water influence”, a concept used in different places through the text.

3.2. Tidal signals and the Mediterranean vein

The time series of velocity and temperature have been low-pass filtered (cut-off period of 3.5 days) in order to investigate subtidal variability. A useful indicator of this variability is the local variations of temperature oscillations at tidal frequencies (mainly M2) in stations of depths #3 and #4. These variations are related to vertical advection of temperature according to

$$\frac{\partial T}{\partial t} = -w \frac{\partial T}{\partial z} \quad (2)$$

if heat diffusion and horizontal advection in the equation of thermal energy are neglected. Both conditions are satisfactorily met for semidiurnal frequencies since diffusion is weak at these time-scales and horizontal tidal excursions are of order of 1 km. The internal tide in this region is dominated by the first baroclinic mode (García Lafuente et al., 2006) which implies that w has the same sign throughout the water column. Therefore M2 oscillations of temperature at two different depths are in phase if the vertical gradient of temperature has the same sign at both depths. Fig. 2 shows that the gradient in A3 and B3 is prone to be negative due to the temperature inversion introduced by the MV, while the gradient at the three other depths is clearly positive. The location of level #3 between the local minimum of temperature above and the local maximum below makes the sign of the gradient at this depth (and, hence, the phase of M2 temperature oscillations) be sensitive to small displacements of the position of the MV.

Fig. 6 shows the tendency of M2 voices in depths #3 and #4 to be out of phase, indicating that A3 and B3 were most of the time in the depth range of negative temperature gradient between the local minimum associated with the ENACW and the local maximum of the MV. This situation is eventually interrupted by periods of nearly-null phase difference (see for instance days around the middle August and the end July – beginning of August in Fig. 6A and C, respectively), during which stations at depth #3 should be close to the local extremes (either minimum or maximum) of temperature. Sharp changes of the phase differences are accompanied by a strong reduction of the amplitude of M2 voices at A3 and/or B3, a fact that could be explained either by the temporal damping of the internal tide or by the proximity of the station to the temperature extremes where vertical displacements of isopycnals hardly changes the local temperature. The persistence of high amplitude of M2 voice in depth #4 (Fig. 4) supports the second possibility whose origin would be connected with the variability of the path followed by the MV (see Fig. 7). This figure shows a vertical section of temperature and salinity

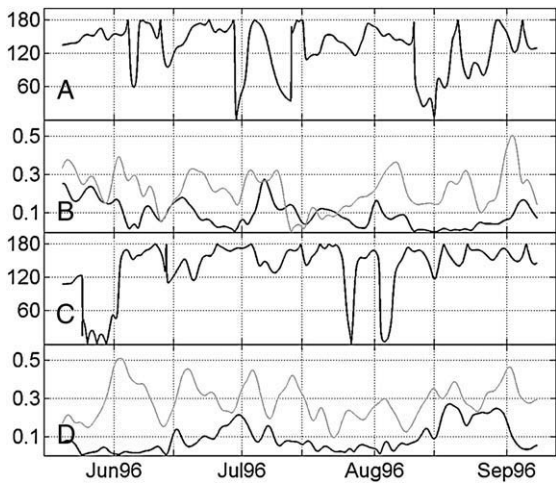


Fig. 6. Panel A: Phase difference (degrees) of M2 voices between stations A3 and A4 (A3–A4). Panel B: Amplitude of M2 voices ($^{\circ}\text{C}$) in A3 (black line) and A4 (grey line). Panel C: Phase difference (degrees) of M2 voices between stations B3 and B4 (B3–B4). Panel D: Amplitude of M2 voices ($^{\circ}\text{C}$) in B3 (black line) and B4 (grey line).

sampled in March 2003 along 43°N , half degree south of site A. Although it is not simultaneous with our measurements and the position is slightly to the south, the spatial distribution of temperature and salinity is thought to represent the circulation of the MV in this latitude reasonably well, with

a narrow core flowing close – but not attached – to the continental slope and a second core west of Galicia Bank. Similar patterns have been reported in the literature (Daniault et al., 1994). A sinking or/and an offshore withdrawal of the core would leave stations at depth #3 in the vicinity of the temperature minimum, reducing the amplitude of M2 voice and changing its phase. Large downwards (upwards) displacements can leave stations at depth #4 (depth #3) near the temperature maximum of the MV, causing similar reductions of M2 voice amplitude. The low-passed temperature series (Fig. 8) will help distinguishing both possibilities. For instance, what happened in site A by the middle of August would have been caused by a noticeable upraising of the MV that would have left A3 close to its maximum (high temperature – Fig. 8, low M2 amplitude – Fig. 6B). On the contrary, the mentioned event in site B by the end of July–beginning of August would correspond with a sinking/withdrawal that would have left B3 close to the minimum (low temperature – Fig. 8 and low M2 amplitude – Fig. 6D).

3.3. Mean pattern and long-term – seasonal – variability

Time-averaged velocity is poleward in all stations under the influence of the MV, the rather moderate maximum of 2.9 cm s^{-1} being found in station A4 where the mean direction is northwards (Table 1). In site B the mean direction is northeast and similar at both depths. This result together with the vertical profiles of Fig. 2, which reveals the typical shape of Mediterranean water at these depths in sites A and B,

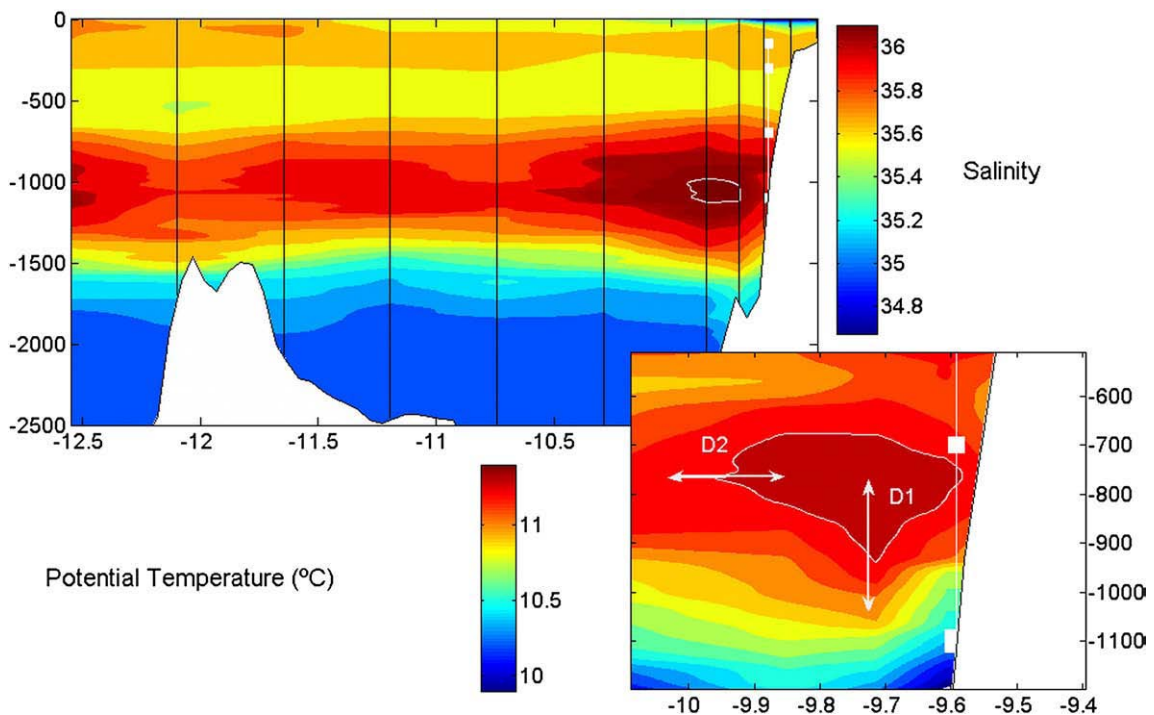


Fig. 7. Vertical profiles of salinity and temperature along 43°N from CTD casts (black lines in the upper panel) accomplished during HIDROPRESTIGE-2003 survey carried out by the Instituto Español de Oceanografía from March 26 to April 6, 2003. White contour in the upper panel is $S > 36.08$ and represents the main core of the MV, which flows close to the continental slope. Lower panel is a close up of this core showing the temperature distribution, the white contour indicating $T > 11.30\text{ }^{\circ}\text{C}$. Solid rectangles near the continental slope show the depths of the instruments and the arrows sketch the possible independent displacements of the vein.

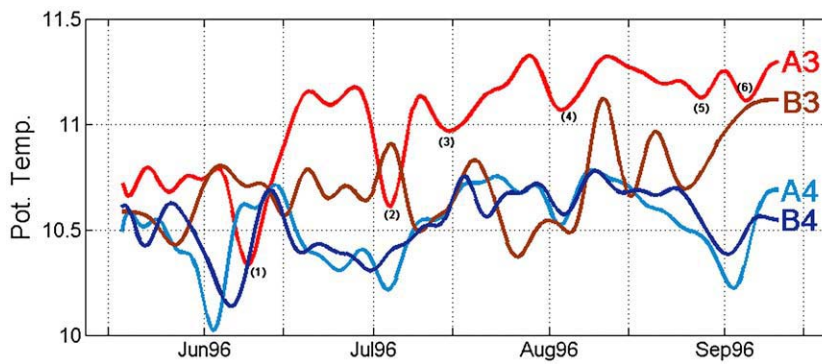


Fig. 8. Low passed temperature series in stations at depths #3 and #4 in sites A and B. Numbers in brackets beside local temperature minima in A3 refer to events mentioned in the text.

indicate that the MV turns anticyclonically around the north-west tip of the Iberian Peninsula in its poleward path, as mentioned in previous works (Iorga and Lozier, 1999). At level #3 both the mean speed and mean temperature diminish downstream while at depth #4 the mean temperature is nearly the same but the mean speed diminishes. Two interpretations can be put forward: the erosion of the temperature as the vein proceeds poleward and mixes with the overlying ENACW and/or the possibility that the core of the MV flows more separated from the continental slope in site B. The decrease of the relative maxima of temperature and salinity from A to B indicated in panels of Fig. 2 (panel A versus panel B; panel C versus panel D) supports the first interpretation, although does not discard the second one.

Vertical profiles of temperature and salinity presented in Fig. 2 show remarkable differences in the depths under the influence of the MV from May to September. These CTD datasets do not allow for analysing the time evolution of the flow, which exhibits high mesoscale variability. One question then arises as to whether or not the differences of hydrological structures found during the surveys are the result of a

seasonal variation driven by identifiable mechanisms or it is just a fortuitous realisation of the mesoscale variability observable in Figs. 3 and 8.

All low-passed temperature series have been linearly fitted for short-term trends with the result that stations at depths #1 and #3 have significant (at 95% confidence level) positive trends of $3.8 \cdot 10^{-3}$ and $6.7 \cdot 10^{-3} \text{ }^\circ\text{C/day}$ (A1 and B1) and $5.5 \cdot 10^{-3}$ and $3.7 \cdot 10^{-3} \text{ }^\circ\text{C/day}$ (A3 and B3), stations at depth #4 have a more reduced but still significant trend of $1.5 \cdot 10^{-3}$ and $1.7 \cdot 10^{-3} \text{ }^\circ\text{C/day}$ (A4 and B4) and stations at depth #2 have hardly significant negative trends. The explanation for positive short-term trend in depth #1 is the seasonal warming of the surface layer while the increasing of temperature at depths #3 and #4 can be explained by a progressive approach of the MV core toward the continental slope that would flood these stations with warmer and also saltier water (see Fig. 7 for reference), as suggested by the increased value of salinity maxima in September (compare panels A and C and panels B and D in Fig. 2). The greater trend in depth #3 than in depth #4 would indicate a combination of shoreward and upwards displacement of the MV originated by the ageostrophic advection that takes place in the lateral boundary layer during the settlement of a wind-induced upwelling. Notice that this advection decreases the temperature at depth #2, in agreement with the negative trend found in A2 and B2. According to this interpretation, the MV would be flowing shallower and more attached to the continental slope during late summer than in spring. The vertical migration could be as large as 100 m, as suggested by the noticeable shallower position of the MV in September showed in Fig. 2.

The possibility that the observed changes between both surveys was due to the fact that Mediterranean waters in the ArG had different thermohaline characteristics in the different seasons cannot be addressed adequately with our dataset. Ambar et al. (2002) found slightly different thermohaline features in summer (September) than in winter (January) in the Gulf of Cadiz, the winter salinity values being higher than those found in summer. Contrary to our case, Ambar et al. (2002) sampled the full extension of the Mediterranean vein in that area and therefore, they were able to ascribe the difference to actual seasonal signals linked to the outflow from the Strait of Gibraltar, as analysed in García Lafuente et al. (2007). The sampling in the present study limits to a small area near the eastern boundary and misses a

Table 1

Statistical mean and variance of velocity and temperature at stations in depths #3 and #4

Station	Velocity			Temperature	
	Ms (cm s^{-1})	Md (deg)	V ($\text{cm}^2 \text{ s}^{-2}$)	MT ($^\circ\text{C}$)	VT ($^\circ\text{C}^{-2}$)
A3	2.5	44	37.1 30.2/6.9 (81%)/(19%)	11.02	$5.9 \cdot 10^{-2}$
A4	2.9	89	23.2 10.6/12.6 (46%)/(54%)	10.53	$3.0 \cdot 10^{-2}$
B3	1.9	20	17.8 15.7/2.1 (88%)/(12%)	10.71	$3.4 \cdot 10^{-2}$
B4	1.3	27	12.8 11.4/1.4 (89%)/(11%)	10.52	$2.1 \cdot 10^{-2}$

Ms and Md are the mean speed and direction (anticlockwise from east) of the flow, V is the variance, representative of the eddy kinetic energy. MT and VT are temperature mean and variance, respectively. Numbers separated by slashes in the velocity variance column indicate the amount of variance in the along-shore/across-shore components of the velocity. Percentages are written below.

large extent of Mediterranean water that is flowing by the ocean interior. However, the MV in the ArG is detected flowing noticeably shallower by the end of summer, a fact that strongly supports the interpretation that the local thermohaline variations are due to the upward-inshore advection of the vein and not to global seasonal changes of the thermohaline characteristics of the Mediterranean water.

3.4. Mesoscale variability

Further to the hypothesised seasonal variability, the time series in Figs. 8 and 9 are dominated by mesoscale variability. The variance of velocity series, which is an estimation of the eddy kinetic energy, diminishes from site A to site B and from depth #3 to depth #4 (Table 1). These values are comparable to those reported in Daniault et al. (1994) at 37°49.9'N, 9°30.6'W, water depth 1110 m ($77 \text{ cm}^{-2} \text{ s}^{-2}$ at 700 m) and at 40°05.2'N, 9°50.6'W, depth 1170 m (25 and $22 \text{ cm}^{-2} \text{ s}^{-2}$ at 700 and 1000 m, respectively). The eddy kinetic energy found in A3 ($37 \text{ cm}^{-2} \text{ s}^{-2}$) is 50% greater than that reported by these authors near 40°N ($25 \text{ cm}^{-2} \text{ s}^{-2}$), which suggests an intensification of the mesoscale activity to the north of this latitude at this depth. At the depth of A4 the eddy kinetic energy maintains similar values.

The strong reduction of more than 50% from site A to site B is probably due to the sheltering effect caused by the orientation of the bathymetry in the latter (Fig. 1). Temperature variance is maximum in station A3 (Table 1), indicating that hydrological variability here is greater than in any other of the remaining stations. This result is not predictable since all stations are located in depths of marked temperature gradient and, consequently, all of them are sensitive to small

changes of water masses circulation. The larger variability in A3 would be partially related to the enhanced eddy kinetic energy found in this station but also to the closeness of level #3 to the relative minimum of temperature associated to the ENACW, as can be concluded from the relatively large temperature variance in B3 compared to the rather reduced eddy kinetic energy in this station (Table 1).

The prevailing direction of the flow is poleward in the four stations (Fig. 9). Around 75% of the time water moves in this direction but there are periodic events that last typically 4 or 5 days during which the flow is equatorward (last days of May, second half of July and August, see Fig. 9). In site B these events happen more frequently, which suggests that the inversion of currents is related to flow instabilities of the MV that would happen north of the area of study, as reported by Paillet et al. (2002) in the case of Meddy Ulla.

The joint analysis of temperature and velocity records depicts a pattern of mesoscale variability coherent with vertical and horizontal displacements of the MV trajectory nearby the observation stations. The local variation of the hydrological properties at depths #3 and #4 can be originated by different processes such as flow instabilities, meddy generation and/or, the most likely to be involved, horizontal (along-shore) displacements or meandering of the MV. The spatial/temporal resolution of the datasets is insufficient to investigate the mechanism behind this variability (more than one could be acting simultaneously), although the analysis of the observations suggests that the seasonal wind-induced upwelling plays a significant role in the observed variability at the depths of the MV.

The analysis is based on the footprint that the displacements of the MV indicated by arrows D1 and D2 in Fig. 7

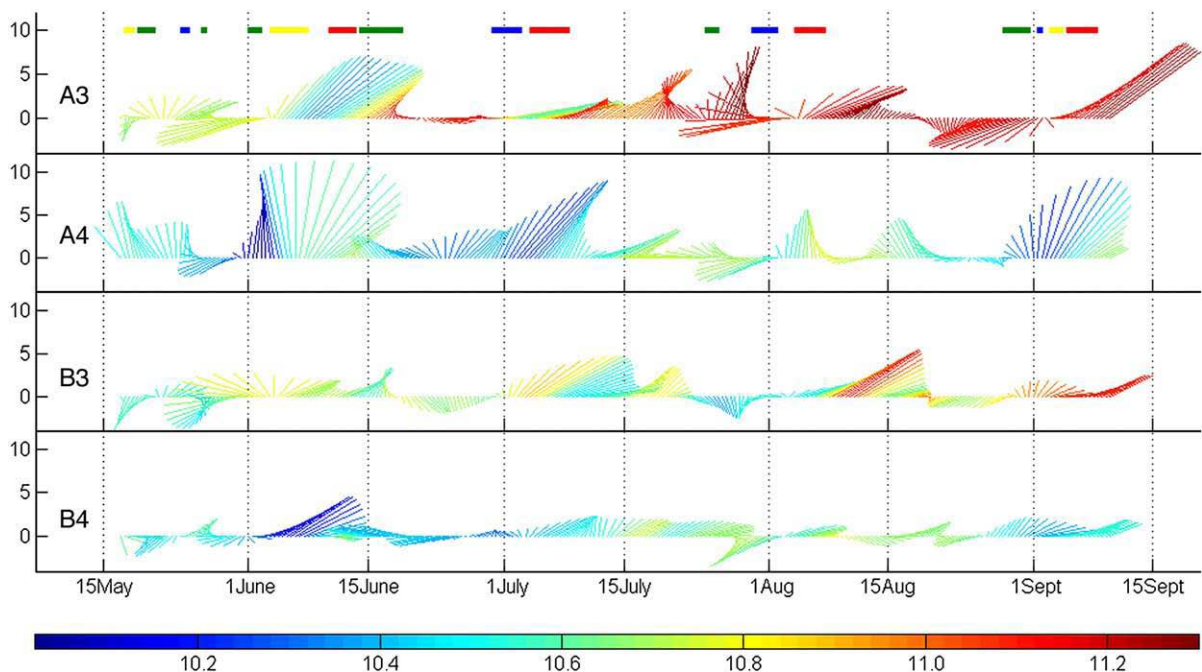


Fig. 9. Stick diagram of the low-passed velocity series in stations at depths #3 and #4 in sites A and B. The colour of the sticks indicates the temperature according to the colorbar in the bottom of the plot. The coloured bars on top of the diagram indicate events of rapid changes of temperature in stations A3 and A4 (see text for details).

would leave in the temperature records. An upwards (D1) displacement of the near-shore core increases the temperature in depth #3 and decreases it in depth #4, inducing changes of different sign. The almost permanent phase opposition of temperature oscillations at M2 frequency between stations at depths #3 and #4 (Fig. 6) indicates that these vertical displacements are the rule for short time-scales. In contrast, the horizontal drifts indicated by arrow D2 would produce temperature changes of the same sign in both stations. Coloured bars on top of Fig. 9 identify events during which the local temperature changed noticeably in A3, in A4 or in both. The events have been identified by computing $\partial T/\partial t$ in both depths, then multiplying the derivatives and selecting the time periods when the absolute value of the product was above the mean plus 0.5 standard deviation. Blue colour identifies events when temperature decreased simultaneously in both depths. According to the previous interpretation, it would be indicative of a D2-type offshore displacement (MV core displaced to the ocean interior). Red colour identifies periods of simultaneous temperature increase that would therefore correspond with a D2-type inshore displacement, the core approaching the continental slope. Green (yellow) colour indicates temperature increase in A3, decrease in A4 (decrease in A3, increase in A4) and would correspond with upward (downward) D1-type displacement.

During the first part of the period most of the temperature variability would have been caused by vertical drifts of the MV (green and yellow colours). The first days of June a remarkable downward displacement would have taken place, making the temperature in A3 fall below the values in A4, a situation never repeated again. It reached the absolute minimum of 10.33 °C (Fig. 8), suggesting that A3 remained for days near the local minimum associated with ENACW. The sharp phase change of M2 voice these days along with its very small amplitude in A3 (Fig. 6) support this interpretation. Shortly after and according to the colour code, an important inshore drift of the MV followed by a marked upwards displacement would have taken place. From then on, temperature in A3 remained above 11 °C (except for a short period by the first days of July when the code in Fig. 8 suggests an offshore drift of the MV, see Fig. 9) and the main source of mesoscale variability would correspond to horizontal drifts of the MV, indicated by the blue and red bars. It is interesting to notice the reasonably good agreement between the colour code and the direction of the flow represented by the sticks. Red colour coincides with periods of inshore component of the velocity vector while blue colour tends to happen in periods of offshore (except for the event in the beginning of July). Obviously the displacements of the MV shall be combination of both basic (D1 and D2) motions, a fact that complicates the interpretation of temperature fluctuations, so that the previous description would only indicate the type of motion with greater influence on these fluctuations during events of rapid change of temperature.

3.5. Horizontal and vertical coherence

The interpretation of the observations in site A is only partially applicable to the stations in site B. There are marked differences such as the largely reduced eddy kinetic energy and temperature variance in the time series or the almost null

cross-shore velocity at this site (Table 1). Flow inversions, that is, water flowing equatorward in depths of Mediterranean water influence where motion is expected to be poleward, are more frequent in station B4 than in A4.

In spite of these facts, there are recognisable similarities in the velocity and temperature fields that support the existence of horizontal coherence. In depth #3, the along-shore components of the velocity, which account for 81% and 88% of the mesoscale velocity variability in stations A3 and B3 (Table 1), respectively, are well correlated at zero-lag ($r=0.70$, $P<0.001$). The same is true for stations A4 and B4 ($r=0.60$, $P<0.001$), showing that the horizontal scale of coherence in the downstream direction is clearly larger than the distance between the stations. Across-shore components at the same depths are not correlated at 95% significance level, a fact that does not appear to be relevant since this component represents less than 20% of the energy in 3 out of 4 stations. Fig. 8 anticipates a good temperature correlation between stations in depth #4 ($r=0.79$, $P<0.001$ at 2-day lag, station A4 leading B4) and a poor and negative correlation between stations at depth #3 ($r=-0.31$, $P<0.005$). This is a surprising result taking into account the rather good correlation of the along-shore velocities between stations A3 and B3.

Comparison of stations in site A indicates good vertical correlation ($r>0.65$) of the velocity field in both along and across-shore directions, with station A4 leading station A3 by 1 or 2 days, and a diminished correlation of temperature ($r\sim 0.5$) at a greater lag (6 days earlier in A4). In site B the along-shore component of the velocity correlates quite well at both depths ($r=0.76$, $P<0.001$) at 2.5 days lag (B4 leading B3) but neither across-shore components, nor temperatures are correlated. The sign of the vertical lagged correlation indicates that mesoscale signals in the velocity field reach first the near bottom station and then progresses upwards with a time scale of two days to cover the 300 m separating levels #3 and #4.

One result that can be extracted from this analysis is that station B3 behaves differently from the remaining stations, particularly regarding temperature fluctuations. The differences could be consequence of the location of site B relative to the local orientation of the isobaths that run from southwest to northeast, leaving stations B3 and B4 partially sheltered from the northward MV. If so, the flow of Mediterranean water would be monitored better in site A where isobaths run in the north-south direction typical of western Iberia, making the flow be less influenced by bottom topography. However, the good correlation found between stations B4 and A4 indicates that sheltering cannot be the only mechanism producing differences. It seems as if the Mediterranean water in site B was flowing deeper than depth B3 and therefore this station was under the influence of the colder and fresher ENACW for longer periods than station A3, which on the contrary seems to be immersed in Mediterranean water most of the time. The frequent and relatively extended periods during which the temperature in B3 was the lowest or nearly the lowest recorded by any instrument (end of May, middle of June, large portions of July and August, see Fig. 8), which moreover coincided with periods of very small amplitude of M2 voice (Fig. 6D), support this hypothesis. Only at the end of the series the station seems to be definitely under the direct influence of the MV (Fig. 8).

3.6. Wind forcing

The most distinguishable feature of the year-round circulation of water masses along the western Iberian coast is the establishment of the seasonal upwelling whose greatest influence is in the surface layer, although it also reaches deeper layers through Ekman pumping. Near the eastern boundary, the offshore Ekman transport during upwelling-favourable wind will be accompanied by upward and/or shoreward ageostrophic velocities in the interior of the eastern boundary layer due to mass conservation. The width of the layer is scaled by the internal radius of deformation, which is $R_i=29$ km for the stratification corresponding to the vertical profiles showed in Fig. 2. According to this scaling sites A and B are inside the lateral eastern boundary layer (assuming that it begins in the continental shelf break) and therefore are sensitive to the upwelling dynamics. Next discussion focuses on site A that, according to Section 3.5, is more suitable to follow the MV fluctuations.

Fig. 10A shows the stick diagram of winds at $42^{\circ}30'N$, $10^{\circ}0'W$ from ECMWF during the period of study. Prevailing wind direction is from the northeast. The lagged correlation between temperature in A3 and the wind component along this prevailing direction (negative for equatorward wind) is remarkable for 14-day delay (Fig. 10B). It has the expected

negative sign: upwelling-favourable wind (negative component) will raise isopycnals in the interior of the boundary layer and bring the core of the MV closer to A3, which will increase the temperature, while wind-relaxation or downwelling-favourable episodes, denoted by bracketed numbers in Fig. 10A, will stop and/or reverse the upraising, cooling the water in A3 (Fig. 8; numbers would correspond to wind events labelled in Fig. 10A). A worth mentioning fact is that during the periods of upwelling relaxation, wind stress curl changes from positive to negative.

Previously to the beginning of the time series in May, winds were not upwelling-favourable but weak and variable. Northerlies started blowing persistently the last days of May and they went on blowing along the whole summer with short episodes of relaxation, whose already commented footprint in the temperature records is exhibited some days later. The intensity of the upwelling-favourable wind increased from the second half of June until the end of July and it was probably this intensification that took the core of the MV close to station A3 and maintained it there for most of summer, a fact supported by the approach of the temperature registered there to the maximum associated with the MV (compare values in Fig. 8 with the numbers in Fig. 2). The weak amplitude of M2 voice during July and, particularly, August (Fig. 6) suggests that A3 was near a relative extreme of

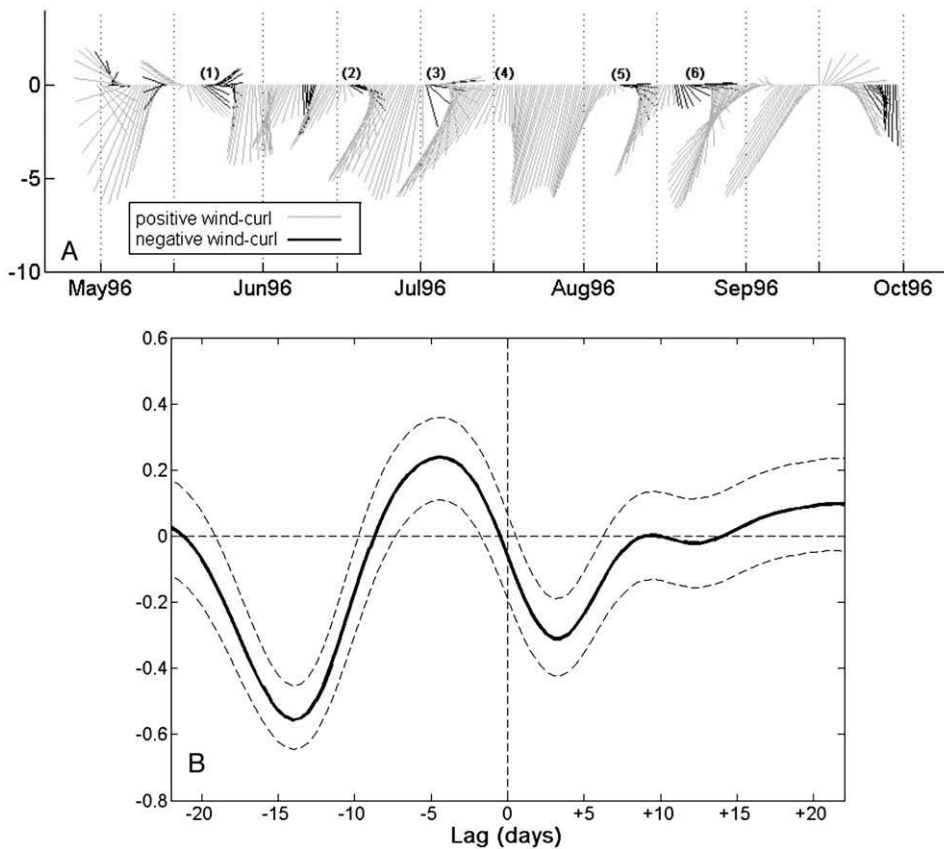


Fig. 10. A) Stick diagram of the wind field in the grid-point $42.5^{\circ}N$, $10.0^{\circ}W$. Scale is $m s^{-1}$. Wind stress curl has been computed from the adjacent grid points and its sign has been indicated in the diagram using the colour code specified in the legend. Numbers in brackets refer to the same events as in Fig. 8. B) Lagged correlation between temperature in station A3 and the wind component along the direction of the mean wind velocity (northeast to southwest). Equatorward wind is negative. Dotted lines are the 95% confidence limits for the correlation.

the temperature profile in this period (a relative maximum in this case), a situation that results in almost null temperature fluctuations at tidal frequencies.

4. Summary and conclusions

Field observations acquired in the ArG during 1996 at the depths of Mediterranean water influence suggest fluctuations of the MV at different time-scales. The noticeable first mode baroclinic M2 tide in the area along with the fact that stations in depth #3 (700 m) are usually above the local temperature maximum associated with the MV while those in depth #4 (1100 m) are below, provides a tool to investigate the meso-scale variability of the vein that complements the direct observations of velocity and temperature fields. The method consists in extracting the M2 voice of the temperature observations using the S-transform (Stockwell et al., 1996; Emery and Thompson, 1997) and compute its slowly-varying amplitude and phase, which are sensitive to the position of the MV in the water column. Stations A3 and B3 are prone to stay near local temperature extremes for extended periods, which implies reduced amplitude of M2 voices. These situations are met either when the MV displaces downward and/or offshore, which would leave level #3 near the temperature minimum associated to ENACW (first half of June in A3 or repeated events in July–August in B3, are examples of this situation) or when it moves upwards and/or inshore to leave level #3 near the local temperature maximum of the MV (most of the second half of July and the whole August provide examples of this situation in A3).

The comparison of CTD observations in May and September indicates a significant warming of water in levels #3 and #4 that has been interpreted as the progressive uprising and shoreward drift of the MV during the upwelling season. Trends computed from temperature time series confirm this warming which, on the other hand, does not take place in a continuous and smoothed manner but following marked fluctuations that have been related to surface wind stress. If observations of year 1996 are representative of the MV dynamics in the area, the Mediterranean water may flow as much as 100 m shallower by the end of the summer (and of the upwelling season) than in spring.

Superposed to this seasonal warming, the observations indicate important mesoscale variability of the vein that leaves characteristic footprints in the records of velocity and temperature. The detailed analysis of the events indicates that the observed fluctuations can be easily explained by a combination of horizontal and vertical drifts of the vein around the yearly-averaged depth and position it flows through. At the beginning of the register, drifts were more probably vertical but they were progressively modified by superposing horizontal drifts that seemed to prevail during summer. Wind stress acting on the surface layer propagates its influence to the deep layer in a delayed mode and shows a significant correlation (and of the expected sign, $r = -0.56$, $P < 0.001$) with temperature in A3, suggesting that a large part of the observed mesoscale variability in the depths of Mediterranean water influence is driven by the successive episodes of upwelling-favourable winds that set up the upwelling regime along the western Iberian coast in summer. This wind-response analysis has been done with stations in site A where

fluctuations of the MV are easily followed, since site B remains topographically sheltered from the main path of the vein due to the change of isobaths orientation in the northwestern corner of the Iberian Peninsula.

Acknowledgments

This work has been partially funded by INGRES projects (REN03-01608/MAR and CTM06-02326/MAR). We are indebted to the crew of BO Francisco de Paula Navarro for his work during the surveys. J.C. Sánchez Garrido acknowledges a grant from the Consejería de Innovación, Ciencia y Empresa (Junta de Andalucía, Project RNM 968) and A. Sánchez-Román a FPI grant from the Spanish Ministerio de Ciencia y Tecnología (ref. no. BES-2004-5530). We acknowledge the deep revision made by two anonymous reviewers of a previous version of this manuscript.

References

- Ambar, I., Howe, M.R., 1979. Observations of the Mediterranean outflow. II The deep circulation in the vicinity of the Gulf of Cádiz. *Deep Sea Research* 26, 555–568.
- Ambar, I., Serra, N., Brogueira, M.J., Cabeçadas, G., Abrantes, F., Freitas, P., Gonçalves, C., Gonzalez, N., 2002. Physical, chemical and sedimentological aspects of the Mediterranean outflow off Iberia. *Deep-Sea Research*. Part 2 49, 4163–4177.
- Ambar, I., Serra, N., Neves, F., Ferreira, T., 2008. Observations of the Mediterranean Undercurrent and eddies in the Gulf of Cadiz during 2001. *Journal of Marine Systems* 71 (1–2), 195–220.
- Baringer, M.O., Price, J.F., 1997. Mixing and spreading of the Mediterranean outflow. *Journal of Physical Oceanography* 27 (8), 1654–1677.
- Bower, A.S., Armi, L., Ambar, I., 1997. Lagrangian observations of Meddy formation during a Mediterranean undercurrent seeding experiment. *Journal of Physical Oceanography* 27, 2545–2575.
- Castro, C.G., Pérez, F.F., Holley, S.E., Ríos, A.F., 1998. Chemical characterization and modelling of water masses in the North East Atlantic. *Progress in Oceanography* 41 (3), 249–279.
- Cherubin, L., Carton, X., Paillet, J., Morel, Y., Serpette, A., 2000. Instability of Mediterranean water undercurrents southwest of Portugal; effects of baroclinity and of topography. *Oceanologica Acta* 23, 551–573.
- Cunningham, S.A., Haine, T.W.N., 1995. Labrador sea water in the Eastern North Atlantic. Part I: a synoptic circulation inferred from a minimum in potential vorticity. *Journal of Physical Oceanography* 25, 649–665.
- Daniault, M., Mazé, J.P., Arhan, M., 1994. Circulation and mixing of Mediterranean Water west of the Iberian Peninsula. *Deep-Sea Research*. Part 1 41 (11–12), 1685–1714.
- Díaz del Río, G., 2006. Patrones hidrológicos y variabilidad temporal de la circulación oceánica en la región plataforma/talud del Golfo Artabro, noroeste de Galicia. Ph.D. thesis, 187 pp., University of Vigo, Vigo, Spain (in Spanish).
- Emery, W.J., Thompson, R.E., 1997. *Data Analysis Methods in Physical Oceanography*. Pergamon Press, 505 pp.
- Fiúza, A.F.G., Macedo, M.E., Guerreiro, M.R., 1982. Climatological space and time variation of the Portuguese coastal upwelling. *Oceanologica Acta* 5, 31–40.
- Frouin, R., Fiúza, A.F.G., Ambar, I., Boyd, T.J., 1990. Observations of a poleward surface current off the coasts of Portugal and Spain during winter. *Journal of Geophysical Research* 95, 679–691.
- García Lafuente, J., Díaz del Río, G., Sánchez Berrocal, C., 2006. Vertical structure and bottom-intensification of tidal currents off Northwestern Spain. *Journal of Marine Systems* 62, 55–70. doi:10.1016/j.jmarsys.2006.04.006.
- García Lafuente, J., Sánchez Román, A., Díaz del Río, G., Sannino, G., Sánchez Garrido, J.C., 2007. Recent observations of seasonal variability of the Mediterranean outflow in the strait of Gibraltar. *Journal of Geophysical Research* 112, C10005. doi:10.1029/2006JC003992.
- Harvey, J., 1982. θ -S relationships and water masses in the eastern North Atlantic. *Deep-Sea Research* 29, 1021–1033.
- Haynes, R., Barton, E.D., 1990. A poleward flow along the Atlantic coast of the Iberian Peninsula. *Journal of Geophysical Research* 95, 11425–11442.
- Haynes, R., Barton, E.D., Piling, I., 1993. Development, persistence and variability of upwelling filaments off the Atlantic coast of the Iberian Peninsula. *Journal of Geophysical Research* 98, 22681–22692.

- Iorga, M.C., Lozier, M.S., 1999. Signatures of the Mediterranean outflow from a North Atlantic climatology. 1. Salinity and density fields. *Journal of Geophysical Research* 104 (C11), 25985–26009.
- Mazé, J.P., Arhan, M., y Mercier, H., 1997. Volume budget of the eastern boundary layer off the Iberian Peninsula. *Deep-Sea Research. Part 1* 44, 1543–1574.
- Paillet, J., Le Cann, B., Serpette, A., Morel, Y., Carton, X., 1999. Real-time tracking of a Galician Meddy. *Geophysical Research Letters* 26, 1877–1880.
- Paillet, J., Le Cann, B., Carton, X., Morel, Y., Serpette, A., 2002. Dynamics and evolution of a Northern Meddy. *Journal of Physical Oceanography* 32, 55–79.
- Peliz, A.J., Fiúza, A.F.G., 1999. Temporal and spatial variability of CZCS-derived phytoplankton pigment concentrations off the western Iberian Peninsula. *International Journal of Remote Sensing* 20 (7), 1363–1403.
- Stockwell, R.G., Mansinha, L., Lowe, R.P., 1996. Localization of the complex spectrum: the S-transform. *IEEE Transactions on Signal Processing* 44 (4), 998–1001.
- Talley, L.D., MacCartney, M.S., 1982. Distribution and circulation of Labrador sea water. *Journal of Physical Oceanography* 12 (11), 1189–1205.
- Torres, R., Barton, E.D., Miller, P., Fanjul, E., 2003. Spatial patterns of wind and sea surface temperature in the Galician upwelling region. *Journal of Geophysical Research* 108 (C4), 27–31.
- Wooster, W.S., Bakun, A., McLain, D.R., 1976. The seasonal upwelling cycle along the eastern boundary of the North Atlantic. *Journal of Marine Research* 34, 131–141.